Department of Veterans Affairs

Journal of Rehabilitation Research and Development Vol. 32 No. 4, November 1995
Pages 349–360

Stress distribution in the ankle-foot orthosis used to correct pathological gait

Tai-Ming Chu, PhD and Narender P. Reddy, PhD
Department of Mechanical Engineering, New Jersey Institute of Technology, Newark, NJ 07102; Department of Biomedical Engineering, University of Akron, Akron, OH 44325-0302

Abstract—Abnormal motion of the ankle-foot complex presents a major problem in the rehabilitation of stroke patients. These patients often develop drop foot, a problem involving excessive and uncontrolled plantar flexion. An ankle-foot orthosis (AFO) is prescribed to constrain and inhibit this abnormal motion. The purpose of this investigation was to simulate the drop foot problem to determine the stress distribution in the orthosis. A quasi-static 3-D finite element analysis of the AFO complex was conducted using ADINA. Results confirmed the hypotheses that the maximum peak stress occurs in the neck, heel, and side-arc region of the AFO. However, the neck region of the AFO experienced the largest amount of stress. High stress concentration in the neck region observed in the present analysis is consistent with the common clinical observation that AFOs break down in the neck region.

Key words: *ankle joint, ankle-foot orthosis (AFO), biomechanics, computer-aided design (CAD), computer-aided manufacturing (CAM), drop foot, finite element model (FEM), polypropylene, stress distribution, subtalar joint.*

INTRODUCTION

The motion of the foot is mainly governed by two joints, the ankle joint and the subtalar joint (1). The ankle joint (2) is the joint between the talus and the tibia, and the subtalar joint (2,3) is between the talus and the calcaneus (**Figure 1**). Pathological conditions, such as stroke, lead to abnormal rotations at the ankle-foot complex that profoundly affect a person's ability to walk. For example, the drop foot problem developed by the stroke patient involves excessive and uncontrolled motion at the ankle joint, often leading to a toe drag instead of the heel contact motion during gait (4). This toe drag, if uncorrected, may lead to falling due to tripping and/or knee buckling (1). In addition, this toe-drag motion will cause an increase in stresses and ulceration of the forefoot (5).

Ankle-foot orthoses (AFOs) have been prescribed to alleviate the drop foot problem (4) so as to constrain or to inhibit excessive plantar flexion (**Figure 2**). In the current clinical rehabilitation applications, the AFOs are generally produced from a variety of thermoplastic materials, such as polypropylene, and are custom fabricated and fitted to the patient (6,7). However, this process is based on the experience and judgment of the orthotist. The material used and the method of fabrication play a major role. The casting and the modification of the orthotic devices is done using trial and error procedures (6,7). There is about a two-to-one ratio for fractures in custom-made orthoses as compared to prefabricated devices (6). Problems such as these not only cause pain and discomfort, but profoundly affect a person's ability to walk and cause reluctance in wearing the orthosis.

Studies on the biomechanics of AFOs have begun only recently (8–10). Lenone (8) formulated a lumped parameter mathematical model of an AFO, using beam equations and small deflection theory. Reddy et al. (9) and Lam et al. (10) formulated a two-dimensional (2-D)

Address all correspondence and requests for reprints to: Tai-Ming Chu, PhD, Assistant Professor, Department of Mechanical Engineering, New Jersey Institute of Technology, University Heights, Newark, NJ 07102; e-mail: tchu@oak.njit.edu.

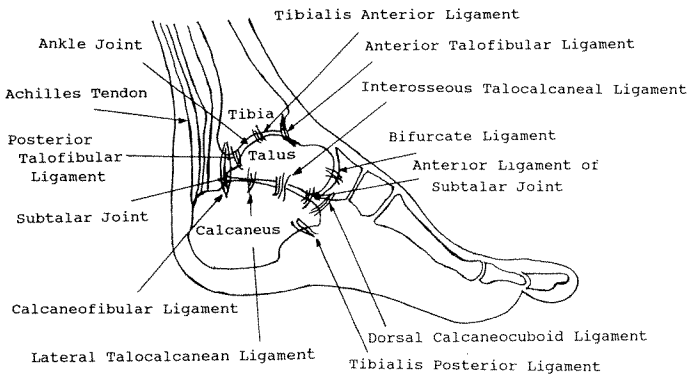

Figure 1.
Schematic representation of the ankle-foot complex.

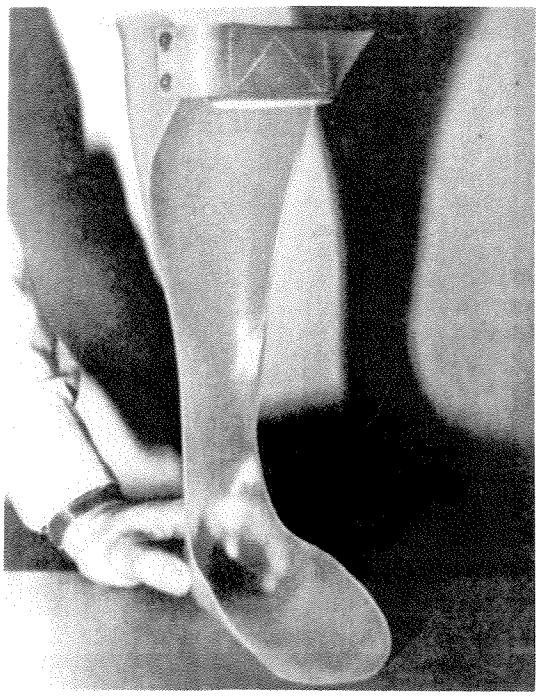

Figure 2.
Polypropylene ankle-foot orthosis (AFO).

model of the AFO complex which assumed symmetry of the device. In reality, orthoses are not symmetrical and cannot be treated by 2-D models. A 3-D finite element model (FEM) has been developed and a static finite element analysis (FEA) of the model conducted (11). However, there continues to be a lack of understanding of the stress distribution in the AFO during gait.

The objective of the present investigation was to study the stress distribution in the AFO during stance phase of the gait using a quasi-static analysis of a 3-D FEM of the AFO complex. This study hypothesized that significant stress concentration in the AFO occurs in the neck and heel regions.

METHOD

A 3-D FEM of a clinically available AFO, together with the ankle-foot system, was developed using the engineering software PATRAN (12) and FEA of the 3-D FEM of the AFO system was conducted using ADINA (13). In particular, the pathological conditions of drop foot were studied. A total of 323 elements and 596 nodes were generated. In general, 3-D eight node isoparametric brick elements were used to represent the AFO, the bones (calcaneus, talus, and forefoot bones), and the soft tissue. Ligaments were simulated by one-dimensional, two node truss elements (**Figure 3**). The orthosis consisted of 128 elements, the soft tissue consisted of 146 elements, the bones consisted of 39 elements, and the ligaments consisted of 10 elements.

The AFO complex was developed from a normal foot (14) and a regular orthotic device (**Table 1**). The model of the foot was assumed to consist of only ligaments, bones, and soft tissue (**Figure 3**). The choice of finite element size and its accuracy were optimized by mesh enrichment. In other words, the model data were checked, before the stress analysis, until the mesh size was close enough to the approximated anatomical data. At the same time, a compromise was made for the data file to be within the allowable range of the computer's capabilities.

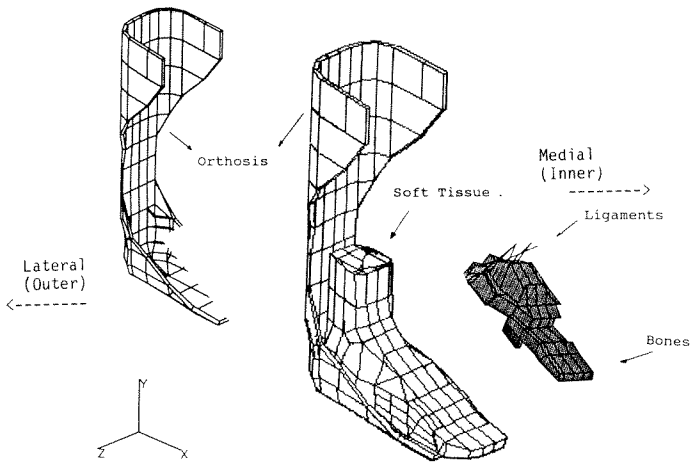

Figure 3.
The finite element model of the ankle-foot orthosis system.

Table 1.
The 3-dimensional anthropometric data of the foot and the orthosis.

		Length (cm)	Width (cm)	Height (cm)	Thickness (cm)	Cross-Sectional Area (cm)
Soft Tissue[1] of the Foot		21.64	7.62	6.40	0.91	
Bones	Talus	2.74	6.71	1.82		
	Calcaneus	4.88	6.71	2.13		
	Other[2]	7.01	6.71	1.82		
Ligaments[3]	DCL	5.48				3.16
	LTL	1.52				3.16
	TAL	9.75				3.16
	TPL	5.48				3.16
	CL	5.79				3.16
	PTL	5.79				3.16
	ITL	1.52				3.16
	ATL	14.02				3.16
	AL	1.52				3.16
	BL	0.91				3.16
Orthosis		16.46	10.06	40.54	0.61	

(1) Soft tissues which surround foot bones; (2) other foot bones, such as the metatarsal bones; (3) DCL = dorsal calcaneocuboid ligament; LTL = lateral talocalcanean ligament; TAL = tibialis anterior ligament; TPL = tibialis posterior ligament; CL = calcaneofibular ligament; PTL = posterior talofibular ligament; ITL = interosseous talocalcaneal ligament; ATL = anterior talofibular ligament; AL = anterior ligament of subtalar joint; BL = bifurcate ligament.

The upper boundary of the leg portion of the 3-D FEM was assumed to be fixed in all planes. This upper boundary was assumed to be at one-third of the height of the normal leg above the ankle joint (**Figure 3**). The upper boundary of the AFO of the 3-D FEM was also constrained to simulate the fact that the AFO was attached to the leg by strapping anterior to the calf. The anterio-plantar aspect of the AFO of the 3-D FEM was extended to the bottom of the foot. This boundary is proximal to the metatarsal heads, at two-thirds of the distance from the heel to the tip of the longest toe (**Figure 3**). It was assumed that there was no slippage between the bones and the soft tissue of the foot, and that no slippage existed between the soft tissue and the bottom flat portion of the orthosis.

The tibia was surrounded by soft tissue and was connected to the foot by ligaments (15–17). The soft tissue was allowed to slip over the tibia without friction in the vertical direction. The tibia-soft tissue interface was constrained in all other directions. The foot bones which form the inner core of the foot in the model were treated as a single structure. The weight of the foot was simulated by the mass proportional loading conditions. Forces exerted in the Achilles tendon and in the flexor and extensor muscle tendons during the foot motion, such as dorsi-plantar flexion, inversion-eversion, and medial-lateral rotation of the foot, were represented by concentrated nodal forces. These forces may not occur at once, and they differ in magnitude and direction during different foot motions.

Also, the ground reaction forces during the heel contact, toe drag (pathological condition), and toe-off during the stance phase of gait were all simulated by concentrated nodal forces. The initial velocity was given to the ground contact point. In this analysis, the material properties for the soft tissue, bones, ligaments, and the polypropylene orthosis were all defined to be linear, perfectly elastic, and isotropic (**Table 2**). The 3-D

Table 2.
Element type and mechanical property of orthosis, ligaments, bones, and soft tissue.

Material	Element Type	Young's Modulus (MPa)	Poisson's Ratio
Ligaments	Truss	$1.15*10^1$	
Bones	3-D Solid	$1.40*10^4$	0.35
Soft Tissue	3-D Solid	1.15	0.49
Orthosis	3-D Solid	$1.03*10^3$	0.43

anthropometric data for the soft tissue, bones, ligaments, and the orthosis are presented in **Table 1.**

For the purpose of the present quasi-static analysis, the velocity of the ground contact point was assumed to be 0.45 m/s at 78° with respect to the x-axis (longitudinal axis of the foot) in the x-y (sagittal) plane (9,10). With the orthosis fixed at the top, the ground contact point was moving up during the heel contact. During normal walking and in corrected drop foot, there is heel contact followed by foot flat and then toe-off. However, to study severe pathological conditions, a toe drag was also simulated with the ground contact point moving up. To simulate the toe-off, the ground contact point had a downward velocity at 100° with respect to x-axis in the x-y plane (9–11).

RESULTS

Significant stress concentrations in the orthosis occurred in the heel and neck regions of the orthosis, and maximum compressive stress in the orthosis occurred during the heel contact (**Table 3**). The maximum compressive stress was located under the heel with the ground contact point located at the center of the heel (**Figure 4**). During the heel contact, a change in ground

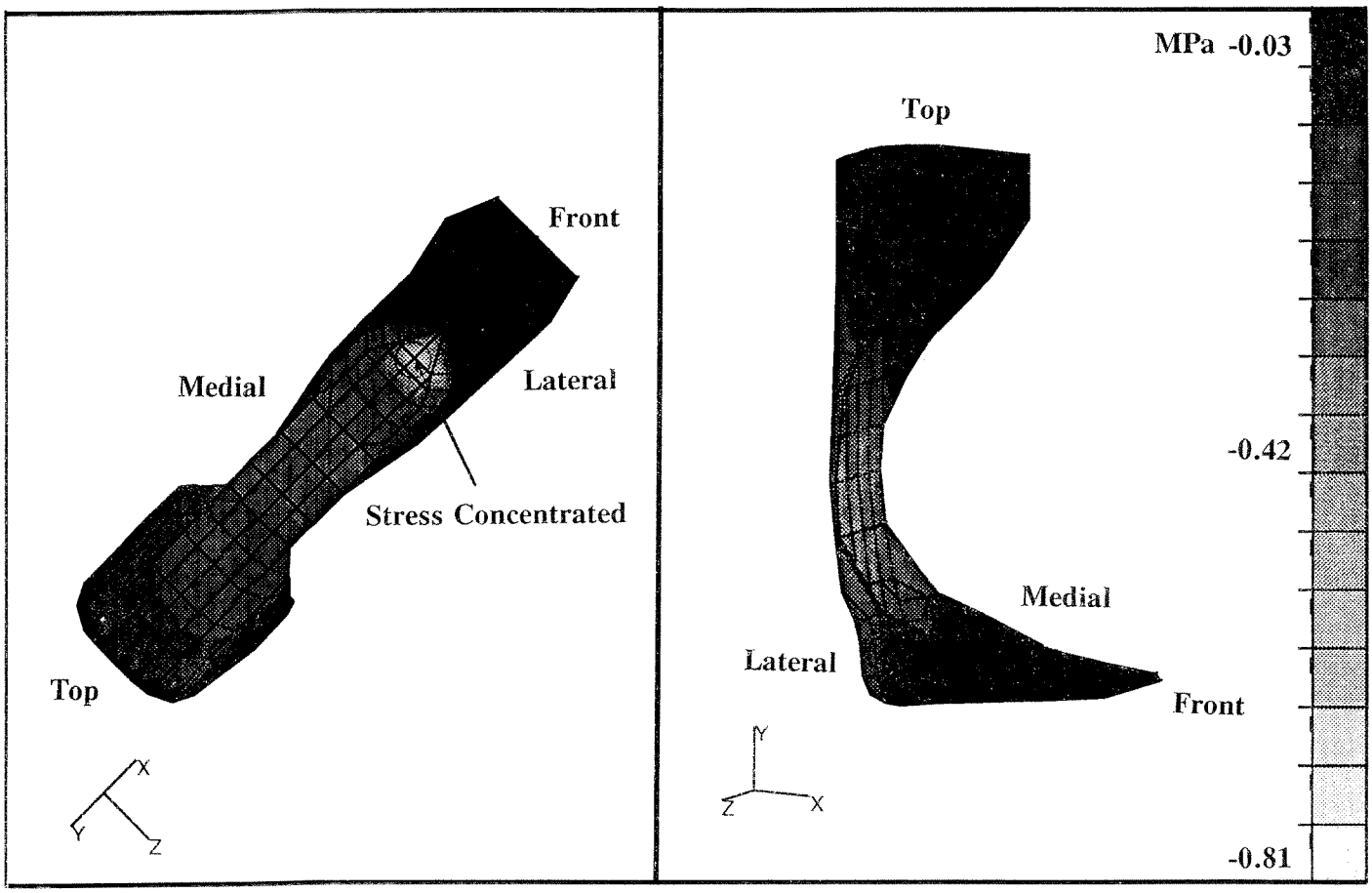

Figure 4.
Compressive stress contours in the orthosis during heel contact in the stance phase with the ground contact point located at the center of the heel (quasistatic analysis). Circled region shows the high stress concentration.

Table 3.
Peak stresses in the orthosis during the stance phase of the gait.

Load Condition and Location(1)			Magnitude of Peak Stress in (MPa) and Its Location in AFO		
Gait	Force	Initial Velocity	Maximum Compressive Stress	Maximum Tensile Stress	Maximum Shear Stress
Heel Contact	HCF @ CH	IV @ CH	0.81 @ Heel	0.11 @ Heel	0.28 @ Heel
	HCF @ LSH	IV @ LSH	1.05 @ Neck	0.28 @ Neck & Side Arc	0.24 @ Neck
Toe Drag	TSF @ MFE	IV @ MFE	0.25 @ Neck	0.45 @ Neck	0.31 @ Neck
Toe Off	TOF @ CFE	IV @ CFE	0.74 @ Side Arc	0.69 @ Neck	0.58 @ Neck
	TOF @ MFE	IV @ MFE	0.80 @ Side Arc	0.80 @ Neck	0.58 @ Neck

(1) HCF = heel contact force (356 N, 78° w/r/t x-axis in the x-y plane); TSF = toe strike force (356 N, 100° w/r/t x-axis in the x-y plane); TOF = toe-off force (356 N, 110° w/r/t x-axis in the x-y plane); IV = initial velocity (0.45 m/s, 78° w/r/t x-axis in x-y plane); CH = center of the heel; LSH = lateral side of the heel; MFE = medial front edge of the orthosis; CFE = center front edge of the orthosis.

contact point from the center to the lateral part of the heel caused an increase in the maximum compressive and tensile stresses and caused a shift in the location of stress concentration from the heel region to the neck region of the orthosis (**Figures 5–7, Table 3**). However, the peak tensile and shear stresses in the model occurred in the neck region during terminal stance at toe-off (**Figures 8** and **9, Table 3**). During the toe-off, the peak compressive stress in the model was located in the medial side arc of the AFO (**Figure 10**). A change in the ground contact point during the toe-off did not cause a change in location of the maximum stresses but caused slight increase in the maximum compressive and tensile stresses (**Table 3**). The toe drag did not cause a significant change in stress distribution in the orthosis (**Table 3**). The peak stresses increased with increased stiffness of the soft tissue and decreased with decreased stiffness of the AFO during the heel contact with the ground contact point located at the center of the heel (**Table 4**).

DISCUSSION

The present quasi-static 3-D FEA confirmed the hypothesis that significant stress concentration in the AFO occurs in the neck and heel regions (11). More specifically, in the present simulation, the peak stresses in the orthosis occurred in the lower neck region (**Figures 6–9**). It is a common clinical experience that the orthoses frequently break down in the neck region (7–11). The results revealed that the AFO experienced significant shear stress and tensile stress during toe-off. There was a 527 percent increase in the peak tensile stress and a 107 percent increase in the peak shear stress during terminal stance at toe-off when compared to heel contact. The locations of the peak tensile and shear stresses changed from the heel region to the neck region during the toe-off when compared to the heel contact. The location of maximum tensile and shear stress concentrations in the neck region during the terminal stance suggest that the AFO exhibits column buckling characteristics. There was a slight (9 percent) decrease in the peak compressive stress during toe-off when compared to the heel contact. The peak compressive stresses occurred during heel contact. Although the location of the peak compressive stress was in the heel region during the heel contact at the center of the heel, the location shifted to the neck region when the heel contact was toward the lateral side of the heel. The significant stress concentrations observed in the neck region of the AFO suggest that the neck region is more susceptible to fatigue breakdown.

The knowledge of the peak stresses can be used to predict the fatigue life of the AFO (18,19). The actual fatigue life depends on the composition and mechanical properties of the orthosis, the fabrication process, activity, and the gait of the individual. The fabrication process and the shelf life also play an important role, and temperature, molding duration, and humidity can significantly alter the properties. Too much temperature can cause hydrogen de-bonding and thus can lead to polymer degeneration. On the other hand, if the temperature is too low, the viscosity of the polymer will be too high, inhibiting the molding process. Moreover, any air bubble formation and sudden cooling during formation of the polymer material can cause significant reduction in the strength. In the present model, homoge-

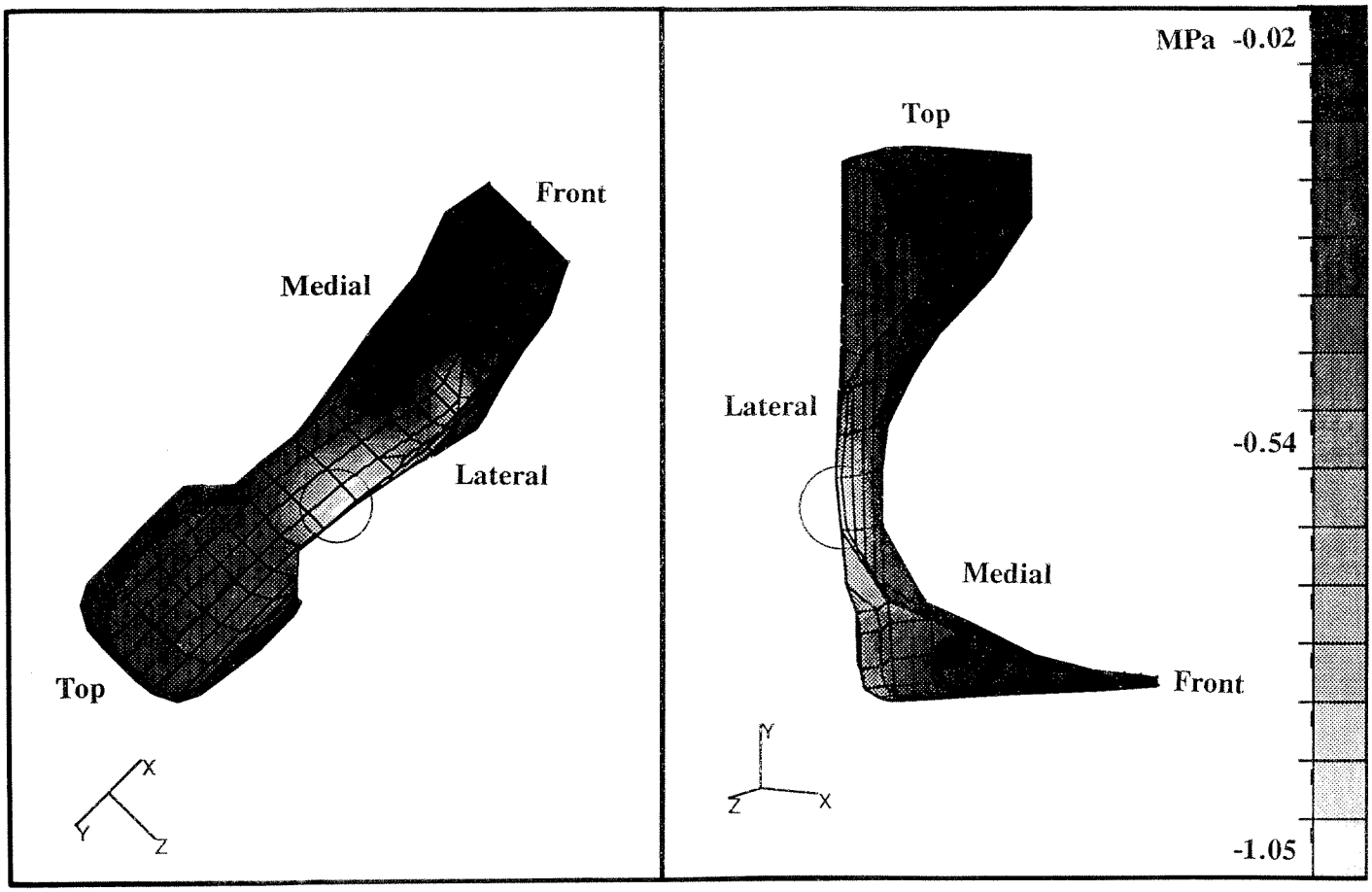

Figure 5.
Compressive stress contours in the orthosis during heel contact in the stance phase with the ground contact point located at the lateral side of the heel (quasistatic analysis). Circled region shows the high stress concentration.

neous and linear properties were used for the AFO. In reality, mechanical properties could be nonlinear or inhomogeneous depending on the molding process. If the material is not properly cured, creep could develop. The present analysis ignores such viscoelastic behavior.

It is a common observation that the frequency of fractures in the custom-made AFO is twice that of the prefabricated device. The effect of material nonlinearities have to be investigated. However, the present linear model will facilitate the development of a PC-based system. The actual fatigue life also depends on the body build and daily activity of the individual. Stair climbing, walking or running (20), and weight lifting can lead to significant stress intensities and decreased fatigue life. In the present analysis, only one velocity, that corresponding to slow walking, was used. The stresses during fast walking and running could be significantly larger. Therefore, the present results provide a relative comparison of the stress distribution in the AFO rather than the actual absolute stress magnitudes.

The parametric analysis revealed that mechanical properties of the soft tissue may play a role in the determination of stress distributions in the AFO. During the simulation of heel contact, a 100 percent increase in the Young's modulus of the soft tissue caused a 39 percent increase in the peak shear stress in the orthosis and 100 percent increase in the peak tensile stress. However, the peak compressive stress did not change significantly (**Table 4**). Moreover, the location of stress concentration shifted from the heel to the neck region of the AFO. The mechanical properties of the AFO play a major role in the determination of stress concentrations. A 20 percent decrease in the Young's modulus of the AFO caused a 30 percent decrease in the peak compressive stress and a 55 percent increase in the tensile stress. The shear stress decreased by 11 per-

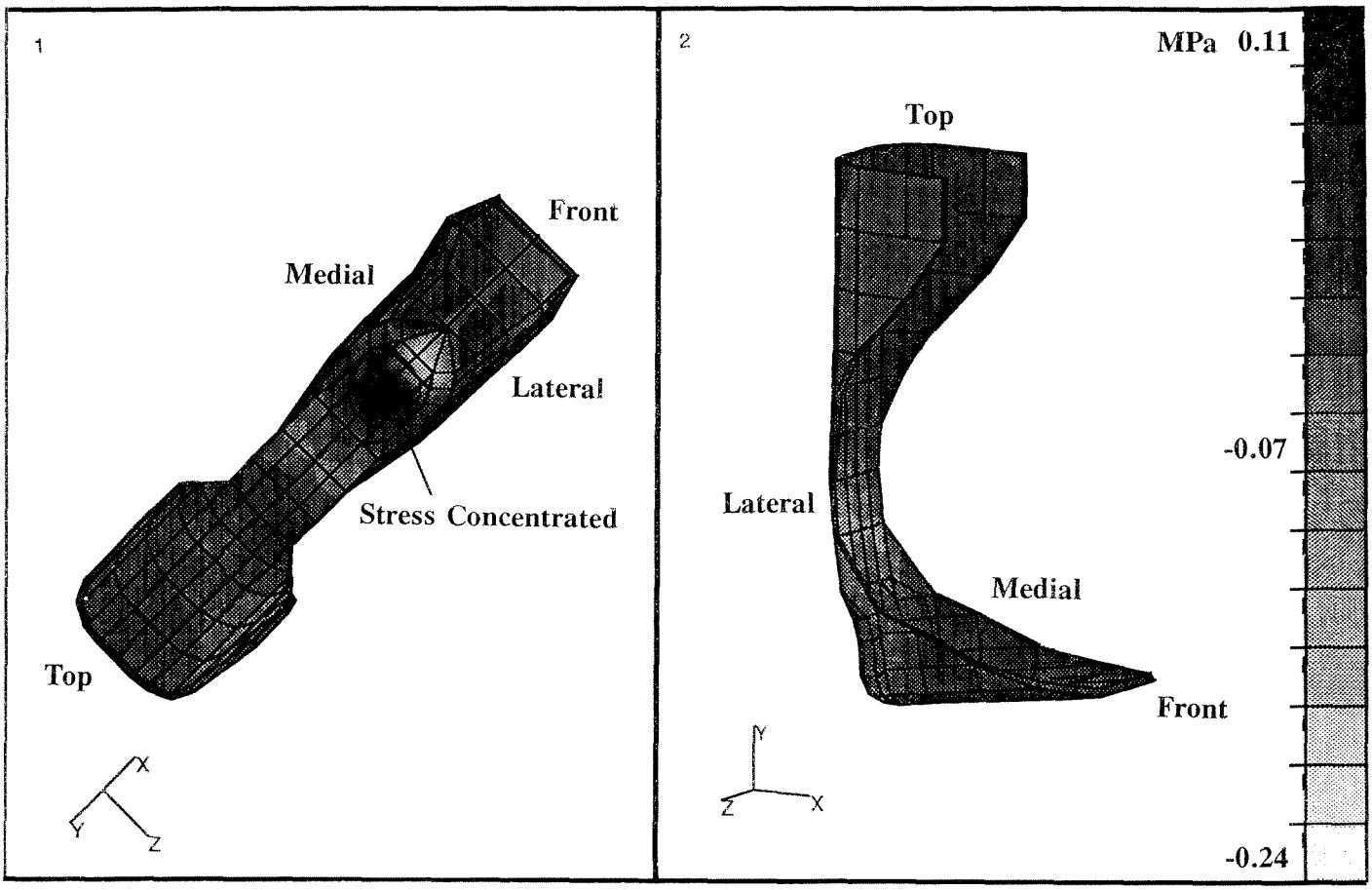

Figure 6.
Tensile stress contours in the orthosis during heel contact in the stance phase with the ground contact point located at the center of the heel (quasistatic analysis). Circled region shows the high stress concentration.

cent. Also, the location of stress concentration changed from the heel to the neck and side arc region of the AFO. These results suggest that the stress distribution in the AFO is more sensitive to the stiffness of the AFO than to the stiffness of the soft tissue. Therefore, significant care should be taken in its manufacture.

The present analysis considered only one type of AFO. There are several other varieties of AFOs, such as the hinge, the NDT, the spring-loaded, the Engin, and so forth. Although the present results are limited to AFOs of relatively identical contour and size, the model could be easily modified to suit other geometries. FEMs could be developed for each type of AFO. Perhaps the present model could be modified for use on a personal computer to facilitate use by the orthotist in a clinical setting. The actual patient geometry can be obtained using MRI, CT Scan, or biplanar radiography, and can be used in the FEA. The mechanical properties of the soft tissue can, perhaps, be estimated from the CT number or by ultrasound. The FEA, together with CAD/CAM, can be used by the orthotist to design, modify, and manufacture the AFOs. In addition, with the advances in polymer technology, it might be possible to alter the local mechanical properties through local irradiation or laser heating. Therefore, the development of a PC-based system may facilitate the design and fitting of orthoses.

In the present analysis, there was no attempt to study the effect of the orthosis on the knee kinematics. Moreover, the mechanical properties in the analysis were assumed to be linear. In reality, the soft tissue is anisotropic, nonlinear, viscoelastic, and discontinuous with several inhomogeneities. Nevertheless, the present model results provide general useful information with

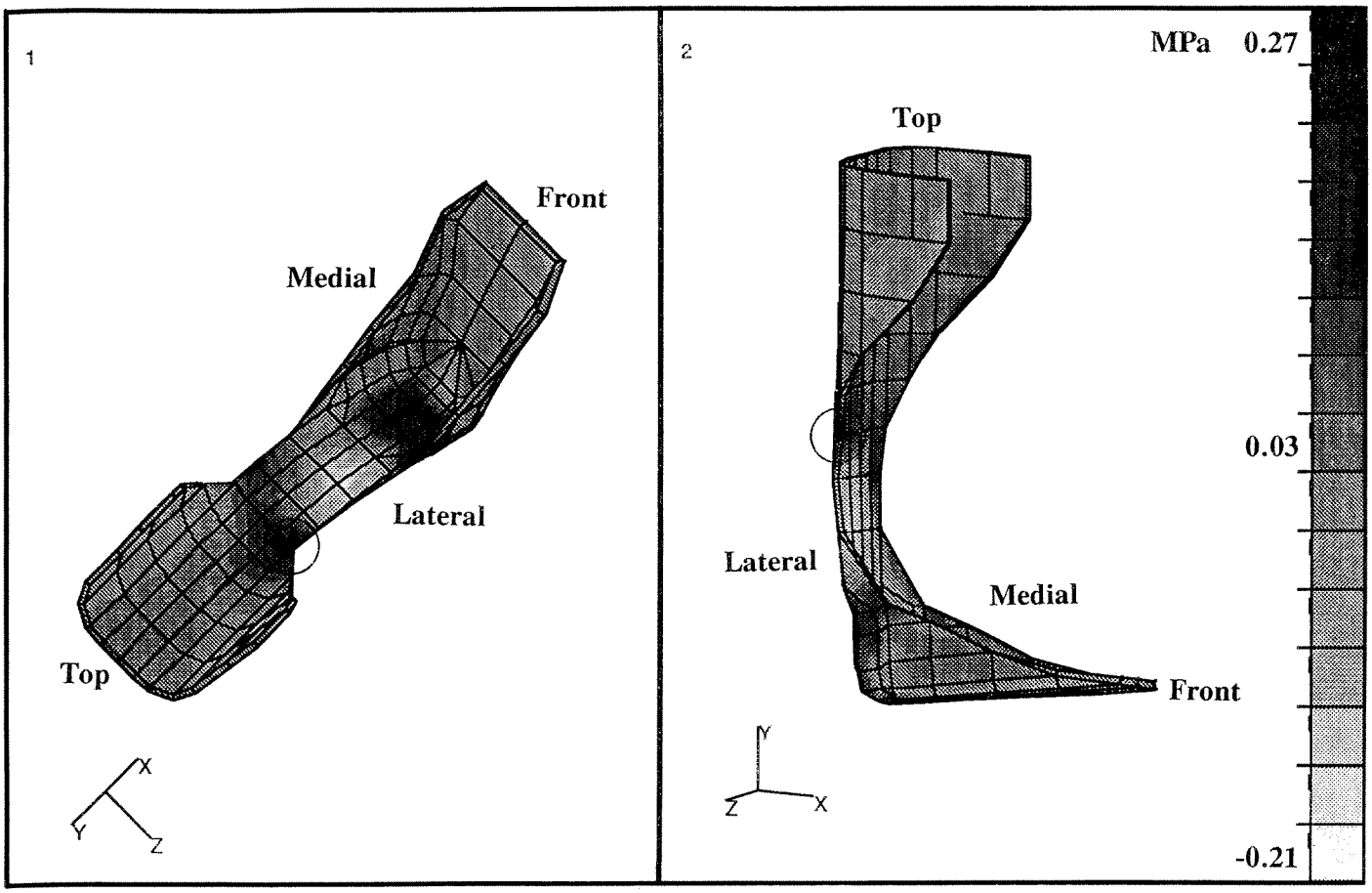

Figure 7.
Tensile stress contours in the orthosis during heel contact in the stance phase with the ground contact point located at the lateral side of the heel (quasistatic analysis). Circled region shows the high stress concentration.

Table 4.
Effect of altered mechanical properties of AFO and soft tissue on the peak stresses in the orthosis.

		Peak Stress (MPa) and Location in AFO		
Material	Parameter (Young's Modulus)	Maximum Compressive Stress	Maximum Tensile Stress	Maximum Shear Stress
Soft Tissue	E_1	0.81 @ Heel	0.11 @ Heel	0.28 @ Heel
	$2 * E_1$	0.88 @ Neck	0.22 @ Neck	0.39 @ Neck
Ankle-Foot Orthosis	E_2	0.81 @ Heel	0.11 @ Heel	0.28 @ Heel
	$0.8 * E_2$	0.57 @ Neck	0.17 @ Side Arc	0.25 @ Neck

The parametric analysis was conducted under the condition of heel contact during the stance phase of the gait.

regard to the types of stresses and stress concentrations developed at various locations in the orthosis.

CONCLUSION

Analysis of the drop foot problem using a 3-D FEM of the AFO has revealed that significant stress concentrations occurred in the neck region of the orthosis. The parametric study of the model suggested that the stress distribution in the orthosis is more sensitive to the stiffness of the orthosis than to the stiffness of the soft tissue.

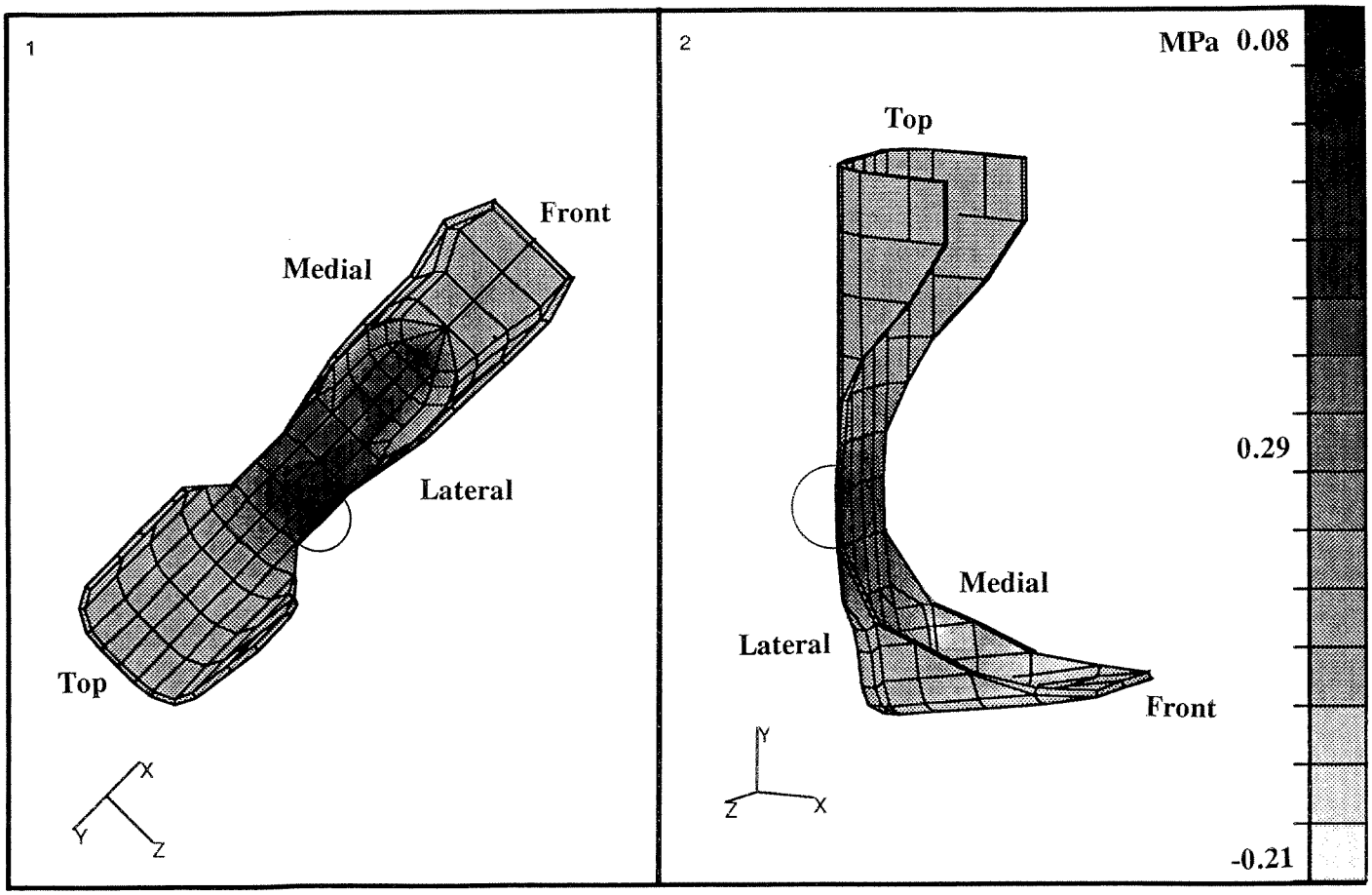

Figure 8.
Tensile stress contours in the orthosis during toe-off in the stance phase with the ground contact point located at the medial front edge of the orthosis (quasistatic analysis). Circled region shows the high stress concentration.

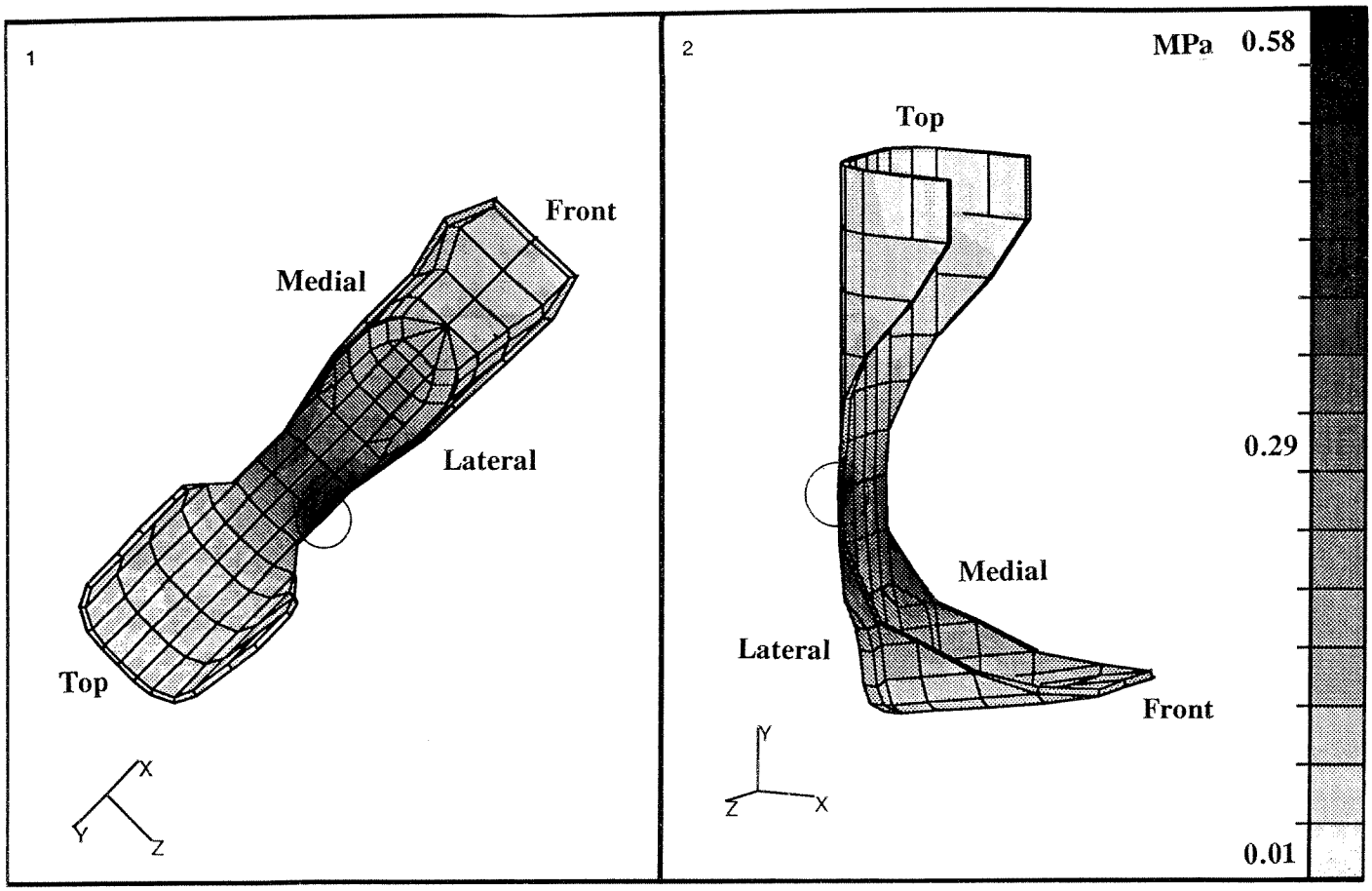

Figure 9.
Shear stress contours in the orthosis during toe-off in the stance phase with the ground contact point located at the medial front edge of the orthosis (quasistatic analysis). Circled region shows the high stress concentration.

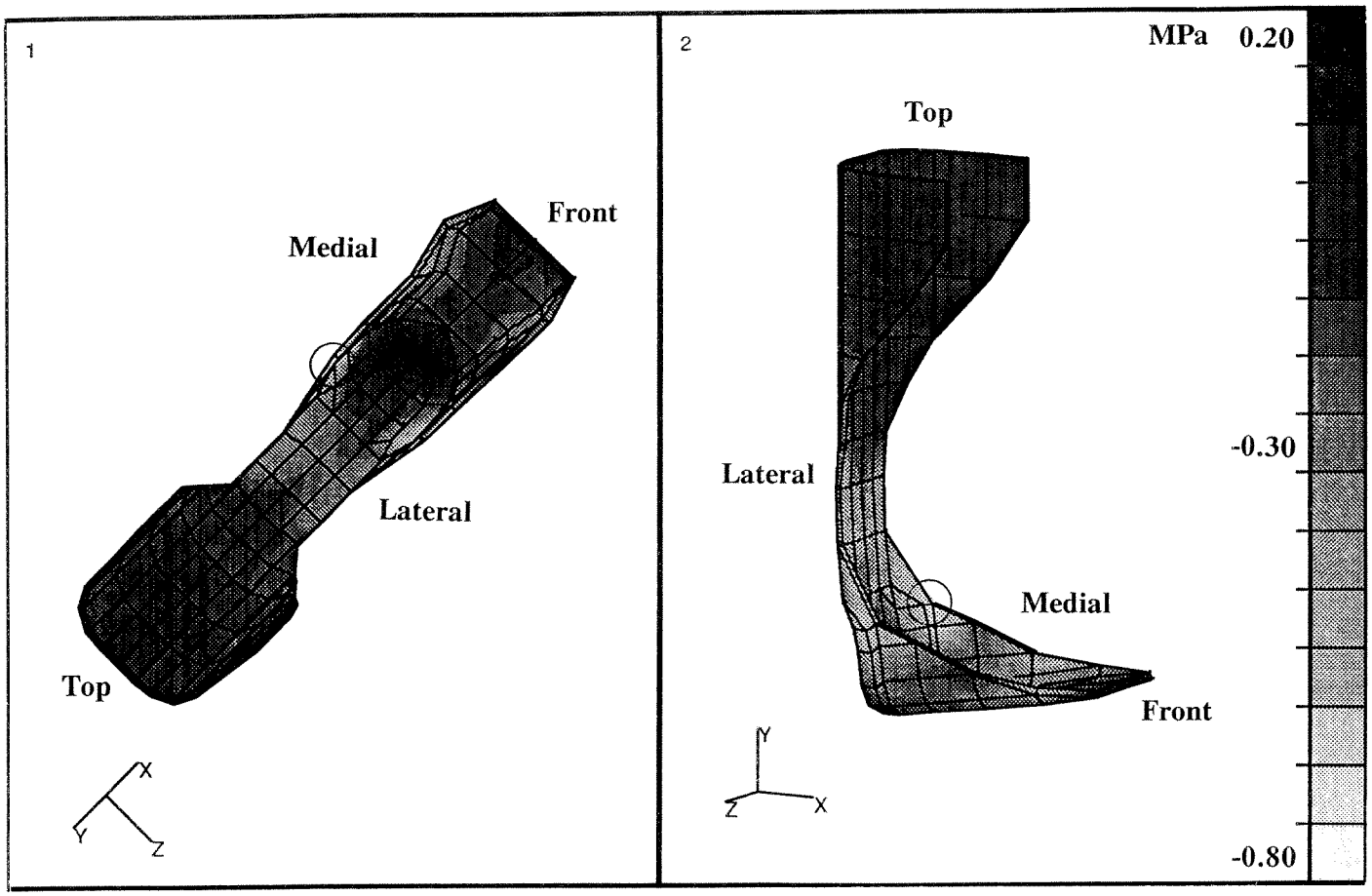

Figure 10.
Compressive stress contours in the orthosis during toe-off in the stance phase with the ground contact point located at the medial front edge of the orthosis (quasistatic analysis). Circled region shows the high stress concentration.

ACKNOWLEDGMENTS

The authors would like to express sincere gratitude to Mr. Mark Yanke, CPO, of Yanke Bionics Inc., for providing the orthosis and for many helpful discussions. Also, thanks are extended to Joseph Padovan, PhD, Distinguished Professor, Department of Mechanical and Polymer Engineering, University of Akron; Thomas W. Findley, MD, PhD, Director of Research at Kessler Institute for Rehabilitation, Enrique P. Canilang, MD, Chairman of Physical Medicine at Edwin Shaw Hospital, and Robert C. Grotz, MD, (formerly of Edwin Shaw Hospital) Director of Heather Hill Hospital, for their encouragement and valuable suggestions for improvement.

REFERENCES

1. Frankel VH, Nordin M. Biomechanics of the ankle. In: Frankel VH, Nordin M, eds. Basic biomechanics of the skeletal system. Philadelphia: Lea & Febiger, 1980:179–91.
2. Inman VT. The joints of the ankle. Baltimore: Williams & Wilkins Co., 1976.
3. Chen J, Siegler S, Schneck CD. The three dimensional kinematics and flexibility characteristics of the human ankle and subtalar joint—part II: flexibility characteristics. J Biomech Eng 1988:110:374–85.
4. Alvin J, Mojica P, Nakamura R, et al. Effect of ankle-foot orthosis (AFO) on body sway and walking capacity of hemiparetic stroke patients. Tohoku J Exp Med 1988:156(4):395–401.
5. Veves A, Murray HJ, Young MJ, Boulton AJM. The risk of foot ulceration in diabetic patients with high foot pressure: a prospective study. Diabetologic 1992:35:660–3.

6. Doxey GE. Clinical use and fabrication of molded thermoplastic foot orthotic devices: suggestion from the field. Phys Ther 1985:65:1679–82.
7. Lehneis HR. Plastic spiral ankle-foot orthoses. Orthot Prosthet 1974:28(2):3–13.
8. Leone DJ. A structural model for molded thermoplastic ankle-foot orthoses. J Biomech Eng 1987:109:305–10.
9. Reddy NP, Pohit G, Lam, PC, Grotz RC. Finite element modeling of ankle-foot orthoses. In: Patil KM, Srinivasan, H, eds. Proceedings of the International Conference on Biomechanics and Clinical Kinesiology of Hand and Foot, Indian Institute of Technology, Madras, India, 1985:95–9.
10. Lam PC, Reddy NP, Downing M. One more step in redesigning the ankle-foot orthosis. SOMA 1987:2(1):36–9.
11. Chu T, Reddy NP, Padovan J. Three dimensional finite element stress analysis of the polypropylene ankle-foot orthosis. Adv Bioeng, ASME, 1992:22:407–9.
12. PATRAN Plus user manual. Costa Mesa, CA: PDA Engineering Software Products Division, 1990:1–2.
13. Users Manual (Report ARD 87-1). Watertown, MA: ADINA R&D, Inc., 1987:1–2.
14. Isman RE, Inman VT. Anthropometric studies of the human foot and ankle. In: Isman RE, Inman VT, eds. Biomechanics Lab. San Francisco: University of California Technical Press, 1968.
15. Rohen JW, Yokochi C. In: Rohen JW, Yokochi C, eds. Color atlas of anatomy, 2nd ed. New York: Igaku-Shoin Co., 1988.
16. Moore KL. In: Moore DL, ed. Clinically oriented anatomy, 2nd ed. Baltimore: Williams & Wilkins Co., 1985.
17. Attarian DE, McCrackin HJ, DeVito DP, McElhaney JH, Garrett WE Jr. Biomechanical characteristics of human ankle ligaments. Foot Ankle 1985:6(2):54–8.
18. Collins JA. In: Collins JA, ed. Failure of materials in mechanical design. New York: John Wiley & Sons, 1981.
19. Sih GC, Provan JW. In: Sih GC, Provan JW, eds. Defects, fracture and fatigue. Boston: Martinus Nijhoff Publishers, 1983.
20. Czerniecki JM. Foot and ankle biomechanics in walking and running. Am J Phys Med Rehabil 1988:1:246–52.